Orientation and Property Correlations for LLDPE Blown Films

H. Y. Chen,[1] M. T.Bishop,[2] B. G. Landes,[2] S. P. Chum[1]

[1]*Dow Plastics, The Dow Chemical Company, Freeport, Texas 77566*
[2]*Core R&D, The Dow Chemical Company, Midland, Michigan 48674*

Received 18 August 2005; accepted 23 October 2005
DOI 10.1002/app.23583
Published online in Wiley InterScience (www.interscience.wiley.com).

SUMMARY: The orientation and property correlations of biaxially oriented polyethylene (PE) blown films have been studied. A linear low density polyethylene (LLDPE) (DOWLEX™ 2045A) was used to fabricate films at different conditions with blow up ratio, die gap, and frost line height as the variables. The White-Spruiell orientation factors of crystal unit cells, amorphous chains, and Herman's orientation factors of lamellae were determined from wide-angle X-ray diffraction pole figure, birefringence, and small angle X-ray scattering (SAXS). A general orientation pattern with the crystal unit cell *a*-axis preferentially oriented to MD, *b*-axis to TD, lamellae stacking along the MD, and amorphous chains preferentially to the MD has been found for all films in this study. A correlation between the orientation of each element of the morphology hierarchy has been revealed. Key mechanical properties including dart impact and Elmendorf tear strength in both MD and TD have been determined. Good correlation has been found among these properties. Most importantly, these properties have excellent correlation to the orientation. These correlations have been linked to underlying morphology and microdeformation mechanisms. © 2006 Wiley Periodicals, Inc. J Appl Polym Sci 101: 898–907, 2006

Key words: polyethylene; blown film; orientation; property

INTRODUCTION

The majority of commercial LLDPE is consumed for film applications. Although different film markets have different performance requirements, superior tear, tensile, and dart impact strength are always desired. It has been recognized that film performance is strongly dependent upon the orientation of both the crystalline phase and amorphous chains, which in turn is largely influenced by the fabrication process and polymer chain microstructure. A clear understanding of the relationships of processing, structure, orientation, and properties is important for future resin design, which includes factors such as branch type, branch content and distribution, and molecular weight and its distribution. Understanding these relationships also gives guidance for film manufacture.

The structure, property, and processing relationships of oriented PE films have been studied for nearly 50 years.[1] However, there are still controversies about the structure of these oriented polymers and they are not fully understood. The *a*-axis structure model was proposed first to explain PE film structure.[1,2] In the *a*-axis structure model, the *a*-axis of the crystalline unit cell for extruded PE films lies along the machine direction. Later, the row-nucleated structure model was proposed by Keller and Machin to give a more comprehensive description of structure development in oriented PE.[3–5] According to their model, two alternative modes of crystallization are possible depending on the stress level in melt. At low stress, the lamellae grow outward from a central nucleation site in the form of twisted ribbons, with their growth axis parallel to the *b*-axis for PE. This crystallization process causes a preferential orientation of the *a*-axis parallel to the machine direction (Keller-Machin Type 1 morphology or *a* texture). At high stress, the lamellae extend radially without twisting, causing the folded chains (*c*-axis) within the lamellae to remain parallel to the molecular chains in the extended microfibers, resulting in the *c*-axis oriented preferentially along the machine direction (Keller-Machin Type 2 morphology or *c* texture). Keller-Machin Type 1 morphology has been found in LDPE, HDPE, and LLDPE films, while the Keller-Machin Type 2 morphology has only been found in some HDPE blown films. However, in some cases, the experimental observations were not fully consistent with row-nucleated structure model, and some modifications of the row-nucleated structure model were also proposed.[6,7] An additional type of morphology has also been found in some PE blown

Correspondence to: H. Y. Chen (hchen@dow.com).
™: Trademark of the Dow Chemical Company.

films, namely a transcrystalline morphology located on the film surface.[8,9]

There have been attempts to correlate the properties of PE blown film to morphology and orientation. Krishnaswamy and Sukhadia found that machine direction (MD) tear strength of LLDPE blown films was higher when the noncrystalline chains were closer to equi-biaxial in the plane of the film, while transverse direction (TD) tear strength was higher when the crystalline lamellae were relatively straight and oriented closer to the TD.[10] Krishnaswamy and Lamborn also explained the differences in tensile properties between MD and TD in terms of both lamellar orientation and organization.[11] Fruitwala et al. correlated MD Elmendorf tear strength to the *b*-axis orientation for both LLDPE and HDPE films.[12] However, a general challenge in reaching a truly satisfactory scientific understanding in morphology–orientation–property studies is that correlation does not necessarily imply causation. Because different hierarchical levels of the morphology are inter-related and thus correlated in a complex way, researchers may focus on a particular measure of orientation and find that it strongly correlates empirically with certain properties; but in fact the true causative explanation for those properties may lie in other structural features.

Many researchers have also attempted to relate the orientation, morphology, and properties to processing conditions. MD/TD stress balance at crystallization,[13,14] flow extension rate in the MD direction,[10] and draw down ratio[15] have been correlated to the morphology and properties of films. The correlation of morphology and properties of blown films to chain microstructure has also been reported. It was found that long chain branching,[16] molecular weight distribution,[17] type of comonomer,[18] and molecular weight[19] can significantly affect the morphology and properties of blown films. The morphology and property differences among HDPE, LDPE, and LLDPE films have also been demonstrated and explained in several recent publications.[20–23] Chain microstructure influences properties both through effects on structure formation (e.g., orientation, morphology) in the blown film process, as well as more direct effects (e.g., lamellar thickness, tie chain concentration).

The current work focused on orientation and property correlations of biaxially oriented PE blown films. A LLDPE polymer (DOWLEX™ 2045A) was used to fabricate films at different conditions with blow up ratio, die gap, and frost line height as the variables. The White-Spruiell orientation factors of crystal unit cells, amorphous chains, and Herman's orientation factors of lamellae were determined from wide-angle X-ray diffraction pole figures, birefringence, and small angle X-ray scattering (SAXS). Key mechanical properties including dart impact and Elmendorf tear in both MD and TD were determined. Correlations between orientation anisotropy and properties are explained in terms of the underlying microdeformation mechanisms.

TABLE I
Processing Conditions Used to Make Blown Films

Run	Blow up ratio	Frost line height (in.)	Die gap(mil)	Drawdown ratio
1	3	40	70	19
2	3	20	70	19
3	2	40	70	29
4	2	20	70	29
5	3	30	100	27
6	3	30	40	11
7	2	30	100	40
8	2	30	40	16
9	2.5	40	100	32
10	2.5	40	40	13
11	2.5	20	100	32
12	2.5	20	40	16
13	2.5	30	70	23

EXPERIMENTAL

Material

The polymer selected for this study was DOWLEX ™ 2045A LLDPE with a density of 0.920 g/cc, and melt index of 1.0 dg/min. This LLDPE is an octene-based copolymer made via a solution process with a Ziegler-Natta catalyst.

Blown film processing

Films were manufactured using a blown film line comprised of a 3.5 in. diameter Sterling extruder (L/D = 32), an 8 in. diameter Gloucester die, an 8.5 in. Saturn II air ring (Future Design Inc.), and a commercial scale film tower. In total, 13 films were produced using a 3-variable Box-Behnken experimental design based around blow up ratio, frost line height, and die gap as the variables (Table I). Processing conditions held constant in this design were melt temperature (425 F), output rate (250 lb/h), and film thickness (1.0 mil). With these constraints, the draw down ratio was another implicit variable in the experimental design.

Film property determination

The Elmendorf tear strength in both MD and TD was measured in basic accordance with ASTM D-1922, but with more stringent criteria on acceptable tests. If the tear path deviated by more than 40°, results were excluded, compared to ASTM D-1922 that allows up to 60° deviation. This was mainly an issue for MD tear for films with low MD tear (up to 15% of specimens

resulted in rejected test results), where deviation of the crack path also corresponded to anomalously high tear strength. Measured tear strengths were normalized by the film thickness to account for small thickness variation. For each direction, 15 samples were measured. Dart impact strength was measured according to ASTM D-1709 (Type A).

WAXD pole figure analysis

For pole figure analysis, 20 layers of films were carefully stacked to enhance 020 diffraction intensity. A stack was made by cutting a long rectangular strip with the length along MD, and spraying adhesive (Elmer's spray adhesive) on the film, and folding the film along the MD. A small piece was cut from the film stack for pole figure analysis.

The R/AXIS-RAPID Curved Image Plate System was used to collect WAXD pole figures. The X-ray radiation (Cu Kα) was produced by using a Rigaku UltraX 18 kW generator. Pole figure data were collected in transmission mode by rotating the films at fixed detector angle ($2\theta \sim 24°$ for the 200 reflection and $2\theta \sim 36°$ for the 020 reflection). Data were collected at angular increments of 5° (χ). An experimentally determined linear background was subtracted from the data for each χ-value.

Small angle X-ray scattering (SAXS)

The SAXS measurements were carried out at the Advanced Photon Source (APS), Argonne National Laboratories. Samples were analyzed in a normal beam transmission mode with a CCD detector that was spatially calibrated with both silver behenate and rat tail tendon standards. Linear representation (one-dimensional plots) of the SAXS data was achieved using the Dow-developed SCATTER visualization and data reduction platform. Plots were generated using both linear and radial integration procedures.

Birefringence measurements

A prism-coupling device, 2010 Prism Coupler manufactured by Metricon, was used to measure the refractive indices of the sample along the MD, TD, and ND. Plane-polarized light was reflected at the prism base at various incident angles. The critical angle of incidence (the angle at which total reflectance occurs) was measured. The critical angle depends on the refractive index of the specimen. Using plane-polarized light and changing the specimen direction (MD or TD), the refractive index was determined along the principal axes of the film (n_M, n_N, and n_T). Birefringence in three orthogonal planes was then calculated from these refractive indices.

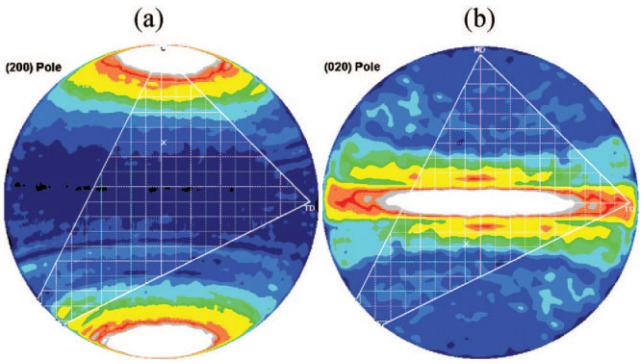

Figure 1 (a) *a*-Axis pole figure and (b) *b*-axis pole figure of the film produced in run eight.[Color figure can be viewed in the online issue, which is available at www.interscience.wiley.com.]

Transmission electron microscopy

The samples were embedded in EPOFIX epoxy and cryo-microtomed at −90 °C along the MD-ND plane. The sections were poststained with RuO_4 for 2 h at ambient temperature. The TEM photographs were obtained with a Hitachi H8100 TEM at 100 kV accelerating voltage.

RESULTS AND DISCUSSION

Orientation at different levels of the hierarchical structure

Crystal unit cell orientation

Crystal unit cell orientation was characterized by WAXD pole figure analysis. Figure 1 contains the (200) and (020) pole figure results for the film produced in run eight. Qualitatively, it is evident that the *a*-axis (200) is preferentially oriented along the MD, because poles with highest intensity are concentrated at the north and south ends of the (200) pole figure. In the (020) pole figure, poles with the highest intensity are concentrated in the center, and spread along the TD. This suggests that *b*-axis is oriented in the ND-TD plane. Essentially similar pole figure patterns were observed for the other films, although of course the orientation and hence the diffraction intensity and spatial intensity distribution in the pole figures varied with processing conditions.

Quantitative orientation factors were determined from these pole figures, starting from calculations of the average squared direction cosines. From the pole figure intensities of (*hkl*) axis (*a*-axis or *b*-axis), it is possible to calculate the average squared cosine angles of the (*hkl*) axis with respect to a direction *i* (MD, TD, or ND) in an orthogonal coordinate MD-TD-ND system by using the following equation:[24]

TABLE II
White-Spruiell Orientation Factors of Crystal Axes and Amorphous Chains, and Herman's Orientation Factors of Lamellae

Run	$f_{a,\mathrm{MD}}$	$f_{a,\mathrm{TD}}$	$f_{b,\mathrm{MD}}$	$f_{b,\mathrm{TD}}$	$f_{c,\mathrm{MD}}$	$f_{c,\mathrm{TD}}$	$f_{am,\mathrm{MD}}$	$f_{am,\mathrm{TD}}$	f_{lam}
1	0.356	0.068	−0.331	−0.167	−0.025	0.099	0.152	0.090	0.530
2	0.459	0.131	−0.451	−0.269	−0.007	0.137	0.141	0.074	0.528
3	0.475	0.035	−0.313	−0.055	−0.162	0.020	0.204	0.082	0.556
4	0.495	0.063	−0.419	−0.177	−0.075	0.113	0.139	0.021	0.553
5	0.441	0.075	−0.355	−0.179	−0.086	0.104	0.143	0.046	0.540
6	0.424	0.090	−0.343	−0.183	−0.081	0.093	0.168	0.060	0.520
7	0.480	0.056	−0.359	−0.133	−0.121	0.077	0.180	0.053	0.563
8	0.391	0.021	−0.283	−0.091	−0.107	0.069	0.175	0.025	0.557
9	0.399	0.073	−0.310	−0.142	−0.089	0.069	0.198	0.102	0.541
10	0.380	0.072	−0.322	−0.160	−0.058	0.088	0.161	0.073	0.532
11	0.433	0.053	−0.325	−0.135	−0.108	0.082	0.171	0.080	0.531
12	0.415	0.065	−0.301	−0.139	−0.113	0.073	0.177	0.057	0.537
13	0.417	0.103	−0.359	−0.197	−0.058	0.094	0.160	0.078	0.529

$$\langle \cos^2 \phi_{hkl,i} \rangle = \frac{\int_0^{\pi/2} I(\phi) \sin \phi \cos^2 \phi d\phi}{\int_0^{\pi/2} I(\phi) \sin \phi \, d\phi} \quad (1)$$

$$I(\phi) = \int_0^{\pi/2} I(\phi,\beta) \, d\beta \quad (2)$$

Because the crystal unit cells in LLDPE blown films are orthorhombic, the orientation of the *c*-axis, in terms of average squared cosine angle can be calculated from those of the *a*- and *b*-axes.

For biaxially oriented materials such as these LLDPE blown films, the orientation functions developed by White and Spruiell are particularly useful.[25] For PE crystals with orthorhombic unit cell, where all three crystallographic axes *a*, *b*, and *c* are of varying lengths and are mutually perpendicular, the White-Spruiell biaxial orientation functions are

$$f_{j,\mathrm{MD}} = 2\langle \cos^2 \phi_{j\mathrm{M}} \rangle + \langle \cos^2 \phi_{j\mathrm{T}} \rangle - 1 \quad (3)$$

$$f_{j,\mathrm{TD}} = 2\langle \cos^2 \phi_{j\mathrm{T}} \rangle + \langle \cos^2 \phi_{j\mathrm{M}} \rangle - 1 \quad (4)$$

The angles ϕ_{jM} and ϕ_{jT} define the orientation of a crystallographic axis *j* (*j* = *a*, *b*, or *c*) relative to the MD and TD axes of the orthogonal MD-TD-ND coordinate system of the film. The orientationally averaged values can be calculated from eqs. (1) and (2). These White-Spruiell biaxial orientation factors range from −1 to + 1.

The White-Spruiell biaxial orientation factors of the *a*-, *b*-, and *c*-axes of the unit cell of the crystalline phase (Table II and Fig. 2) show that all films exhibit preferential orientation of the *a*-axis along the film's MD, and preferential orientation of the *b*-axis in the TD-ND plane with a bias towards the ND. The *c*-axis displays some preferential orientation along the TD; however, the *c*-axis orientation factors along the film's MD and TD are both close to zero, indicating that the *c*-axis is more isotropic than either the *a*-axis or *b*-axis. Note that in the White-Spruiell orientation diagram (Fig. 2), the biaxial orientation factors of the crystal unit cell axes along the MD are plotted versus their counterparts along the TD, and the dotted line represents equi-biaxial orientation in the MD-TD plane of the film. Similar observation was also reported by others. By using an FTIR approach, Krishnaswamy and Sukhadia observed that the *a*-axis in LLDPE blown films was oriented more to the MD and *b*-axis oriented

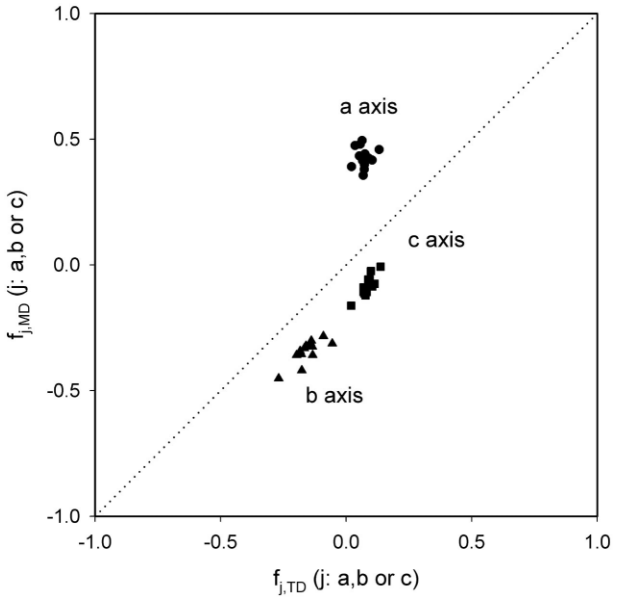

Figure 2 White-Spruiell crystalline biaxial orientation factors.

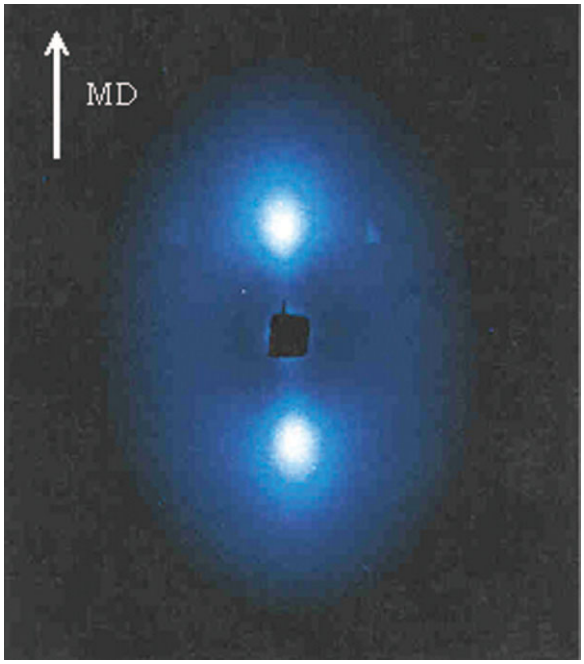

Figure 3 SAXS pattern of the film produced in run eight. [Color figure can be viewed in the online issue, which is available at www.interscience.wiley.com.]

more to the TD.[10] Zhang et al. reported that *a*-axis orientation was along the MD, while *b*-axis orientation was perpendicular to the MD.[21]

Lamellar orientation

SAXS can be used to determine the lamellar orientation and periodicity.[26] The SAXS pattern for film from run 8, for x-ray radiation incident along the ND, is shown in Figure 3. A two-point pattern was observed corresponding to a periodicity along the MD. For all films, a similar pattern was observed. This result indicates that the lamellar normals found in all of the films were preferentially aligned in the MD. This observation is consistent with the WAXD pole figure results. In polyethylene (PE), the *b*-axis lies along the lamellar growth direction. The observation of the *b*-axis orientation along TD/ND plane from pole figure measurement suggests that the lamellar normal was preferentially aligned to the MD.

For this work, only one SAXS pattern (with an X-ray beam perpendicular to the film's surface) was collected for each sample. Using the assumption that the lamellae exhibit axial symmetry with respect to a sample direction, the Herman's orientation factor can be calculated by the following equation:

$$f = \frac{3\langle \cos^2 \phi_{\mathrm{lam},z} \rangle - 1}{2} \qquad (5)$$

where $\phi_{\mathrm{lam},z}$ is the angle between the lamellar normal and a reference axis z, e.g., the MD. The evaluation of $\langle \cos^2 \phi_{\mathrm{lam},z} \rangle$ with respect to the z reference axis can be calculated by eq. (5). Since these films do not possess axial symmetry (they have been biaxially oriented), the Herman's function allows only the determination of relative orientation values within the plane of the films. According to this orientation factor definition, if the lamellae are oriented perfectly along the MD, the value is 1. If all lamellae are oriented to the TD, the orientation factor is -0.5.

Orientation factors calculated from the SAXS data using eq. (5) are listed in Table II. These factors provide only limited information on lamellar orientation, since the biaxial films do not possess axial symmetry. The factors can be used to understand the balance or imbalance of orientation that exists in the plane of the film samples. The orientation factors were in the range of 0.520–0.563, which indicates that lamellae are preferentially stacked along the MD, with a spread of misorientation around this direction.

Figure 4 is the TEM micrograph of the sample produced in run 3. Sample produced in run 3 has the highest orientation. It can be seen that the lamellae have a weak orientation with the lamellar normal more in the MD direction. Although some lamellar stacks with the normal along the MD can be seen, in general, these lamellar stacks are ill-defined and localized. This suggests that, in general, these films do not have well-defined, row-nucleated structure or there are some groups of small lamellar stacks, which are ill-defined, localized row-nucleated structures. Others have also observed that there is no obvious row-nucleated morphology in LLDPE blown films.[21,27] According to the combined observations from WAXD pole figures, SAXS and TEM, it seems that a mixed

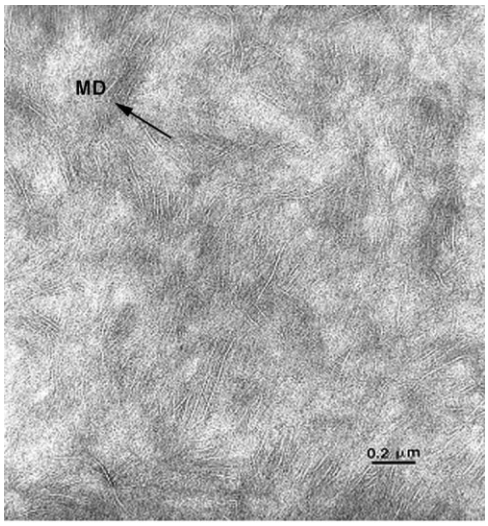

Figure 4 TEM micrograph of the film viewed normal to the MD-TD plane.

morphological model of ill-defined, row-nucleated structure and *a*-axis structure needs to be used to describe the morphological texture.

Amorphous chain orientation

The birefringence, Δ_{ij}, is defined as the difference in refractive index between two perpendicular directions *i* and *j*. It measures the global orientation of the specimen, comprising a combination of crystalline, amorphous, and form birefringence. The form birefringence is often neglected,[9] and the total birefringence is assumed to be the weight-fraction averaged linear combination of crystalline and amorphous contributions. With these assumptions, the amount of amorphous orientation in the blown films can be estimated by the following equations:

$$\Delta_{TN} = n_T - n_N = w[\Delta_{bc}^{oc} f_{c,TD}^{c} + \Delta_{ab}^{oc} f_{a,TD}^{c}] + (1 - w)\Delta^{oa} f_{am,TD} \quad (6)$$

$$\Delta_{MN} = n_M - n_N = w[\Delta_{bc}^{oc} f_{c,MD}^{c} + \Delta_{ab}^{oc} f_{a,MD}^{c}] + (1 - w)\Delta^{oa} f_{am,MD} \quad (7)$$

where $\Delta_{bc}{}^{oc}$ and $\Delta_{ab}{}^{oc}$ are the intrinsic crystalline birefringence for the *bc* and *ab* planes of the unit cell, Δ^{oa} is the intrinsic amorphous birefringence, $f_{am,MD}$ and $f_{am,TD}$ are amorphous biaxial orientation functions. In these equations, $f_{c,TD}^{c}$, $f_{c,MD}^{c}$, $f_{a,TD}^{c}$, and $f_{a,MD}^{c}$ are the same as $f_{c,TD}$, $f_{c,MD}$, $f_{a,TD}$, and $f_{a,MD}$, which were defined in eqs. (3) and (4).

The crystallinity of all blown films as measured by DSC was found to vary little with the processing conditions, so weight fraction crystallinity was taken constant at 0.43. Using this value along with the crystal orientation and birefringence data, amorphous chain orientation factors were calculated according to eqs. (6) and (7). The intrinsic birefringence values of $\Delta_{cb}{}^{oc}$, $\Delta_{ab}{}^{oc}$, and Δ^{oa} used in eqs. (6) and (7) were 0.056, −0.005, and 0.058, respectively.[25]

Values calculated for White-Spruiell biaxial orientation factors are listed in Table II. The results indicate that amorphous chains are preferentially oriented along the MD, although not strongly so. This is consistent with the previous conclusion from a film shrinkage experiment.[17] In that study, it was observed that films shrunk much more in the MD than the TD at temperatures below the melting point, which was attributed to preferential orientation of amorphous chains along the MD.

Correlations between orientation of the different elements of the morphology hierarchy

Figure 5 is the plot of the *b*-axis in-plane orientation factor difference versus the *a*-axis in-plane orientation factor difference. These orientation factor differences represent how anisotropic the crystal axes are in MD-TD plane, and the sign represents whether a particular crystal axis is more aligned with MD or TD. The larger the difference, the more anisotropic. It was found that when the *a*-axis was more aligned to the MD, the *b*-axis was more oriented to the TD. As is well known, the *b*-axis in PE is the lamellar growth (i.e. lamellar long axis) direction. In Figure 6, the difference in *a*-axis orientation factors along the TD and MD are plotted against the lamellar orientation factors determined from the SAXS data. It can be seen that there is a good correlation between how strongly the lamellar normals are oriented to the MD (*y*-axis of Fig. 6) and how strongly the *a*-axis is oriented to the MD (*x*-axis of Fig. 6).

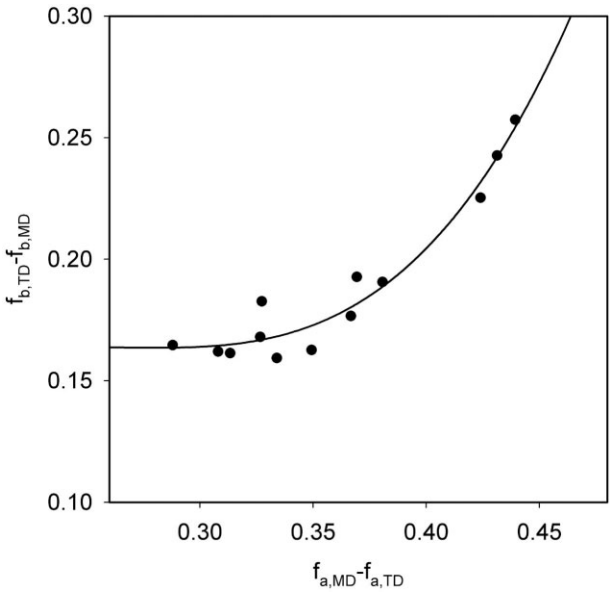

Figure 5 The difference in *b*-axis orientation factors along TD and MD plotted against the difference in *a*-axis orientation factors along MD and TD.

Figure 7 is the plot of the amorphous chain orientation factor difference in two directions versus the *a*-axis orientation factor difference in two directions. The difference represents how much the amorphous chains or crystal *a*-axis are aligned in the MD. The larger the difference, the more oriented in the MD. It was found that when amorphous chains were more aligned to the MD, *a*-axes were more oriented to the MD. This trend suggests that crystalline phase orientation and amorphous chain orientation in PE blown films may both be related to similar process variables. This may be described using the development of row-nucleated structure. As we know, the deformation in the MD is typically greater than the deformation in the TD during blown film processing, as indicated by the large drawdown ratio (Table I). As a result, chains may be preferentially aligned along the MD in the

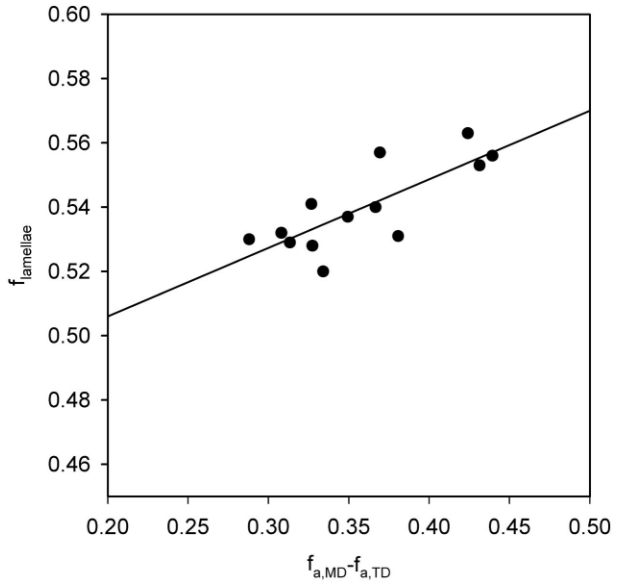

Figure 6 Lamellar orientation factor from SAXS plotted against the difference in *a*-axis orientation factors along MD and TD.

melt. Subsequently, when these chains crystallize, they can epitaxially grow on the pre-existing extended chains radially from this surface. As a result, if amorphous chains were more aligned to the MD, lamellae should be stacked more along the MD. The difference in *a*-axis orientation factors between two directions is greater than the difference in amorphous orientation factors in two directions, which suggests that the crystalline phase orientation is more anisotropic than amorphous chains in the MD-TD plane. This can be explained by the fact that the crystals, once formed, may have limited degrees of translational or rotational freedom because of some degree of interconnectivity, whereas the amorphous chains may be able to relax and randomize to some extent during cooling.

Attempts were also made to correlate the absolute orientation factors of various elements of the morphology hierarchy. However, no good correlation was found. This may suggest that only orientation anisotropies will correlate with each other at the various structural levels, not the absolute orientations. This may occur because the different morphological features under interrogation may each be affected to some extent independently by different process variables. This conclusion that orientation anisotropy is more important than absolute orientation is consistent with prior observations that the ratio of stresses at the freeze point, not the absolute values of the stress, is what governs the morphology that is formed and the anisotropy of the structure.[15]

In the next section, this issue of how the properties of these LLDPE films are related to orientation anisotropy will be explored. Because of the correlations between different orientation anisotropies, it does not fundamentally matter which orientation function is used to correlate to film properties. However, *a*-axis orientation has a practical advantage, in that *a*-axis orientation data have the least experimental uncertainty as compared to *b*-axis, *c*-axis, and amorphous orientation data. The diffraction intensity of *b*-axis is much weaker than that of *a*-axis. As a result, the *b*-axis orientation data tend to exhibit more scatter. The *c*-axis orientation is calculated from *a*- and *b*-axis results and thus has even more uncertainty. The amorphous orientation data have the largest uncertainty, since they are calculated from birefringence and crystal orientation factors and because form birefringence was neglected.

Film properties and property-orientation correlations

Tear strength

Tear strength is one of the most important properties for PE blown films. In Figure 8, MD and TD Elmendorf tear strength are plotted as a function of the difference between the *a*-axis orientation factors in two directions. The difference represents how much the *a*-axes are aligned to the MD relative to the TD. When the difference is zero, *a*-axes are oriented equi-biaxially in the plane of the film. A good correlation was found between tear strength and *a*-axis orientation anisotropy. The MD tear strength decreased, while TD tear strength increased, when *a*-axes were more aligned in the MD. Moreover, when the *a*-axis orientation is closer to equi-biaxial in the plane of the film,

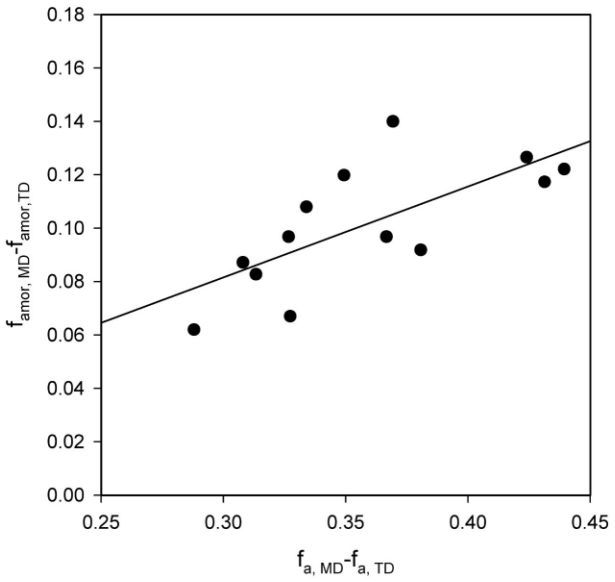

Figure 7 The difference in amorphous chain orientation factors along MD and TD plotted against the difference in *a*-axis orientation factors along MD and TD.

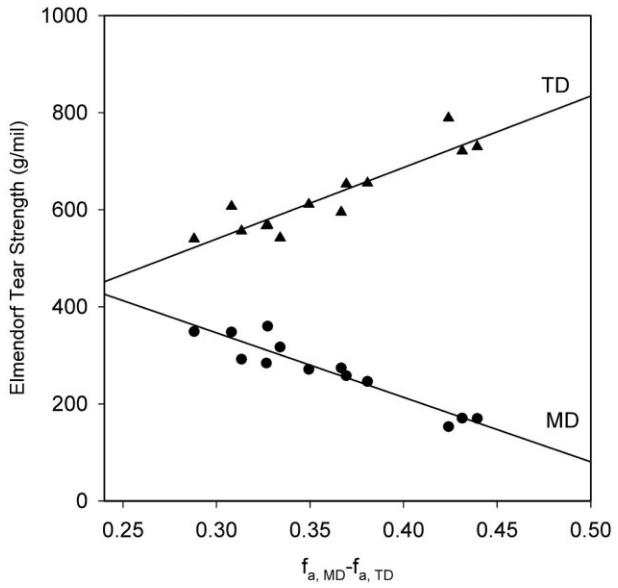

Figure 8 Tear strength correlation to *a*-axis orientation anisotropy in the MD-TD plane.

the tear strength difference between the two directions is the lowest.

This correlation can be explained from the underlying deformation mechanism. Tear strength is the energy dissipated in growing the crack. In these blown films, lamellae are stacked more along the MD. For MD tear, the crack can initiate and propagate either between lamellar stacks or through the lamellar crystals themselves (breaking only van der Waals bonds), resulting in lower energy required for tear propagation.[21,23] For TD tear, greater energy is dissipated during crack propagation because lamellar orientation is not favorable for ease crack initiation and propagation. Instead, other micromechanisms with higher energy dissipation are favored. Because of amorphous chain alignment along the MD in this texture, the amorphous chains will be significantly stretched along the MD, which is indicated by the strong strain hardening in MD tensile experiments.[10] These oriented amorphous chains are probably tie chains between crystalline lamellae. The covalent bonds in the tie molecules would need to be broken for crack propagating along the TD, which is a high energy dissipation process. The important influence of tie chains on the TD tear strength has also been used to explain the difference on the TD tear strength of HDPE, LDPE, and LLDPE films.[23] At a more macroscopic, phenomenological level, lower MD tear corresponds to lower energy to break in TD tensile, and higher TD tear corresponds to higher energy to break in MD tensile. The importance of film stretching to the tear strength was also recognized in Krishnaswamy's work.[10] A perhaps oversimplified explanation of these tear strength differences is that morphology can be simplified as a row-nucleated type structure, although relatively weakly so. Interconnections between the different "rows" are generally weaker than the interconnections along the rows; therefore, propagating a tear in the MD that proceeds more or less between the rows results in a lower tear strength.

The data in Figure 8 and Table III also suggest that when tear strength in one direction is higher, the tear strength in the other direction is lower. These results clearly show the link between anisotropic tear behavior and structural and orientational anisotropy. Low MD tear strength can be a limiting factor for many end-use applications. Improved MD tear strength can be achieved by more balanced orientation or by less orientation. These can be accomplished, for example, by using a higher blow up ratio or a lower draw down ratio.

Dart impact strength

Dart impact strength is another important property for blown films. Figure 9 shows the relationship between dart impact strength and *a*-axis orientation factor difference between the MD and the TD. Dart impact strength decreases as the orientation anisotropy increases. The dart drop impact applies a biaxial tensile load that translates to an anisotropic in-plane biaxial stress state. For anisotropic films, despite an opposed initial stress anisotropy, fracture in dart impact occurs along the MD that is the weaker direction, for reasons that were discussed above in connection with tear strength. It is therefore reasonable and in fact observed (Fig. 10) that dart impact strength increases with increasing MD tear strength which in turn correlates to decreasing orientation anisotropy. When the MD-TD in-plane orientation is equibiaxial, the dart impact strength is the highest. Moreover, it was observed that the shape of broken films after dart impact test was often not circular but elliptical with the long

TABLE III
Mechanical Properties of Films

Run	MD tear (g/mil)	TD tear (g/mil)	Dart impact (g)
1	349	540	552
2	360	568	396
3	170	730	172
4	170	721	154
5	274	595	272
6	317	542	350
7	153	789	156
8	258	653	126
9	284	567	450
10	348	606	466
11	246	655	268
12	271	611	250
13	292	556	406

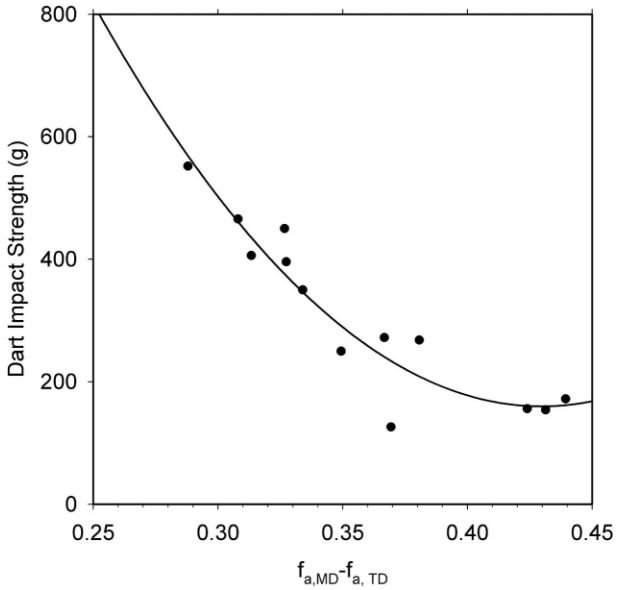

Figure 9 Dart impact strength and *a*-axis orientation anisotropy correlation.

axis along MD. Furthermore, dilatational bands, which were parallel to the MD, were observed at the edge of the unbroken films. The dilatational bands are highly deformed regions of the film, which are closely associated with a mode I crack.[28] These experimental observations suggest that failure in dart impact is predominantly via a crack propagated along the MD. Since the MD tear strength decreases with increasing *a*-axis orientation anisotropy, as discussed in the previous section, the dart impact strength decreases with increasing *a*-axis orientation anisotropy. Thus, to improve the dart impact strength, one should maximize the MD tear strength. This could be accomplished by using a higher blow up ratio or a lower drawdown ratio.

In this paper, we showed how the various measures of orientation anisotropy are strongly correlated with each other. Results suggest that properties are better correlated with orientation anisotropy than with absolute orientation factors. That the orientation and orientation anisotropy of different structural features is interrelated is of course well known. However, despite this knowledge, researchers have often tended to argue that properties are related primarily to the orientation of a specific feature of the overall structure, or to only one of the many variables during film fabrication and structure formation. Most of the references cited in this introduction are examples of this typical mode of interpretation. In contrast to this typical view, we argue that properties are best considered as correlated to the texture as a whole. The observation that properties can be correlated equally well to various orientation factors, each reflecting orientation of a different specific element of the overall structure, supports the hypothesis that properties and property balances are determined by the structure as a whole. This result in turn implies that the most useful explanations of properties are those that are based on the factors that are the strongest determinants of the final overall texture. Phenomenological factors such as the MD/TD stress ratio and crystallization rate—which in turn reflect the complex interplay of molecular variables such as molecular weight distribution and short chain branch distribution with a given set of fabrication conditions—are therefore expected to be the factors most directly related to the morphological structure as a whole, and therefore to properties.

CONCLUSIONS

Orientation and property correlations of biaxially oriented PE blown films have been studied. A linear low density polyethylene (LLDPE) (DOWLEX™ 2045A) was used to fabricate films at different conditions with blow up ratio, die gap, and frost line height as the variables. The White-Spruiell orientation factors of crystal unit cells and amorphous chains were determined from wide-angle X-ray diffraction pole figures and birefringence, and the Herman's orientation factor of lamellae was determined from small angle X-ray scattering (SAXS). A general orientation pattern with the crystal unit cell *a*-axis preferentially oriented to MD, *b*-axis to TD, lamellar stacking along the MD, and amorphous chains aligned preferentially to the MD has been found for all films in this study. This work confirmed the long-standing assumption from shrinkage experiments that amorphous chains in typical LL-

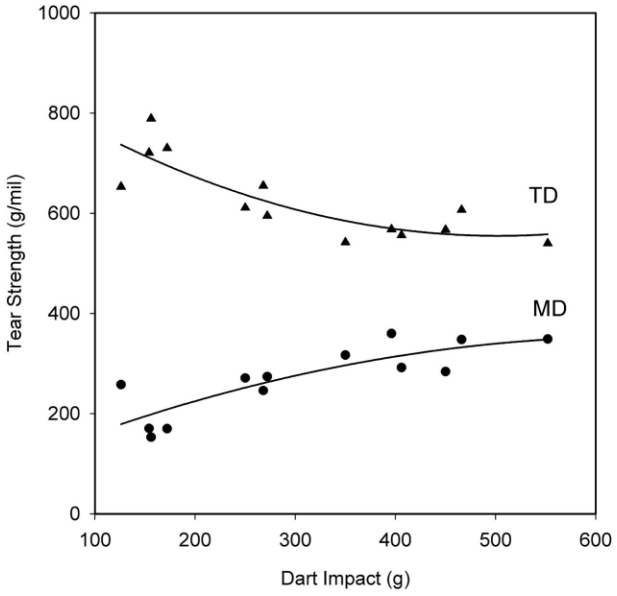

Figure 10 Correlation between tear strength and dart impact strength.

DPE films are aligned preferentially along the MD. Cross-correlations between the orientation and especially the orientation anisotropy of different elements of the morphology hierarchy have been revealed. The existence of strong correlations between different orientation factors explains why different researchers have over the years found good correlation between particular properties against nominally different structural elements for correlation. Key mechanical properties including dart impact and Elmendorf tear strength in both MD and TD have been determined. Good correlations have been found among these properties. Most importantly, these properties show excellent correlation with orientation anisotropy. These various correlations have been justified in terms of the underlying morphology and well-established microdeformation mechanisms. In this study, both orientation–orientation and orientation–property correlations have been found to be stronger with regard to orientation anisotropy instead of absolute orientation. This suggests that the ratio of the stresses during the film blowing process plays a significant role, along with absolute stresses, in establishing orientation, structure, and properties of the final film.

The authors thank C. C. Chau, Craig Dryzga, and Joe Dooley for useful discussions. We also acknowledge the contributions of Tom Butler for making blown films for us, Delrose Winter from AMIA Labs for WAXD pole figure data acquisition and Ralph Guerra for TEM analysis. Lastly, we thank our coworkers in the Fabricated Product Film Testing Lab and the Polyolefin Film Testing Lab for their assistance in measuring film mechanical properties.

References

1. Holmes, D. R.; Palmer, R. P. J Polym Sci 1958, 31, 345.
2. Aggarwal, S. L.; Tilley, G. P.; Sweeting, O. J. J Appl Polym Sci 1959, 1, 91.
3. Keller, A. Nature 1954, 174, 826.
4. Keller, A. J Polym Sci 1955, 15, 31.
5. Keller, A.; Machin, M. J. J Macromol Sci Phys 1967, 1, 41.
6. Desper, C. R. J Appl Polym Sci 1969, 13, 169.
7. Lu, J.; Sue, H. J. Macromolecules 2001, 34, 2015.
8. Maddams, W.; Preedy, J. J Appl Polym Sci 1978, 22, 2721.
9. Pazur, R. J.; Prud'homme, R. E. Macromolecules 1996, 29, 119.
10. Krishnaswamy, R. K.; Sukhadia, A. M. Polymer 2000, 41, 9205.
11. Krishnaswamy, R. K.; Lamborn, M. J. Polym Eng Sci 2000, 40, 2385.
12. Fruitwala, H. P.; Shirodkar, P.; Nelson, J.; Schregenberger, S. D. J Plast Film Sheeting 1995, 11, 299.
13. Choi, K.; Spruiell, J. E.; White, J. L. J Polym Sci Polym Phys Ed 1982, 20, 27.
14. Kwack, T. H.; Han, C. D.; Vickers, M. E. J Appl Polym Sci 1988, 35, 363.
15. Patel, R. M.; Butler, T. I.; Walton, K. L.; Knight, G. W. Polym Eng Sci 1994, 34, 1506.
16. Prasad, A.; Shroff, R.; Rane, S.; Beaucage, G. Polymer 2001, 42, 3103.
17. Simpson, D. M.; O'Neil, D. G. Tappi J 1995, 78, 170.
18. Kim, Y.; Park, J. J Appl Polym Sci 1996, 61, 2315.
19. Sherman, E. S. Polym Eng Sci 1984, 24, 895.
20. Guichon, O.; Séguéla, R.; David, L.; Vigier, G. J Polym Sci Part B: Polym Phys 2003, 41, 327.
21. Zhang, X. M.; Elkoun, S.; Ajji, A.; Huneault, M. A. Polymer 2004, 45, 217.
22. Lu, J.; Sue, H. J Polym Sci Part B: Polym Phys 2001, 40, 507.
23. Lee, L.-B. W.; Register, R. A.; Dean, D. M. J Polym Sci Part B: Polym Phys 2005, 43, 413.
24. Alexander, L. E. X-ray Diffraction Methods in Polymer Science; Wiley-Interscience: New York, 1969.
25. White, J. L.; Spruiell, J. E. Polym Eng Sci 1981, 21, 859.
26. Guinnier, A.; Fournet, G. Small-angle Scattering of X-rays; Wiley: London, 1955.
27. Johnson, M. B.; Wilkes, G. L.; Sukhadia, A. M.; Rohlfing, D. C. J Appl Polym Sci 2000, 77, 2845.
28. Sabbagh, A. B.; Lesser, A. J. J Polym Sci Part B: Polym Phys 1999, 37, 2651.